Noise in Two-Tier Matrix Amplifiers

KARL B. NICLAS, SENIOR MEMBER, IEEE, AND AUGUSTIN P. CHANG, MEMBER, IEEE

Abstract—**A noise theory for the two-tier matrix amplifier [1] has been developed that permits the computation of the amplifier's noise figure as a function of the active device and circuit parameters. The computed results based on the noise parameters of a GaAs MESFET with the gate dimensions 0.25×200 μm are discussed. In addition, a comparative study is done on the performance data of a 2×4 matrix amplifier and its equivalent two-stage distributed amplifier. Finally, the noise characteristics of two 2×4 matrix amplifiers incorporating GaAs MESFET's processed on either ion-implanted or VPE substrate material are compared with those measured on actual amplifiers.**

I. Introduction

THE CONCEPT OF the matrix amplifier, and its practical realization in the form of a 2×4 rectangular array, have been discussed in a recently published paper [1]. The new device combines the processes of additive and multiplicative amplification, along with their characteristic features, high gain and wide bandwidth, in one and the same module. Its two-tier version (two rows of active devices) distinguishes itself from an equivalent two-stage distributed amplifier using the same number and types of transistors by its significantly smaller size and improved reflection coefficients. In addition, an equally or even more important characteristic surfaced when the theoretical noise behavior of the new amplifier was examined. There is reasonable evidence that the matrix amplifier offers a more desirable compromise between its broad-band maximum noise figure on the one hand, and its gain as well as VSWR performance on the other, when compared with an equivalent distributed amplifier. An understanding of the two-tier matrix amplifier's noise behavior and of the influence of its active, as well as passive, circuit elements on the noise figure therefore becomes an important factor in the design of such amplifiers. In addition to a discussion of the device's noise theory and its noise as a function of certain circuit parameters, a comparison between computed results and measured data performed on two different 2×4 array amplifiers is made.

II. The Noise Theory

In this chapter we develop the theoretical basis that ultimately leads to the formula for the noise figure. It is intended for those readers who are interested in the derivation and the validity of our formulas. However, it may be omitted by those who are mainly concerned with the computed results, such as the dependence of the noise behavior on the circuit parameters.

Manuscript received January 17, 1987; revised May 7, 1987.

The authors are with the Watkins-Johnson Company, Stanford Research Park, Palo Alto, Ca 94304.

IEEE Log Number 8717906.

The formulas derived in this paper consider only the noise contributed by the active devices and the thermal noise injected by the terminations of all idle ports. The part that is contributed by the lossy transmission line elements or lossy inductors, as well as capacitors, is considered to be comparatively small and has therefore been neglected [2], [3].

In our efforts to determine the matrix amplifier's noise parameters, we will essentially follow the procedure used for the distributed amplifier which is described in the literature [3]. The generalized circuit diagram of the two-tier matrix amplifier ($m=2$) consisting of n columns of active devices is shown in Fig. 1. For the noise analysis of this amplifier, we divide the module into the same functional blocks as was done in [1], i.e., the input four-port, the linking six-ports, the two-tier active six-ports, and the output four-port. The input and output four-port contain the idle ports' terminations which, as will be seen later, significantly contribute to the noise figure of the device.

A. The Two-Tier Active Six-Port

Fig. 2 presents the circuit of the two-tier active six-port which incorporates the two cascaded transistors as well as the transforming transmission line elements T_{Dmk} and the drain line open-circuit shunt stubs T_{4k} characterized by their π-shaped equivalent circuits and their noise sources as shown in Fig. 3. The latter consist of the noise voltages $v_k^{(A)}$ and $v_k^{(B)}$ as well as the noise currents $i_k^{(A)}$ and $i_k^{(B)}$ located at the input port of each active device in accordance with Fig. 3. The index k refers to the kth elementary six-port. The relationship between the circuit elements $Y_{Fijk}^{(\,)}$ in Fig. 2 and those of the equivalent circuit $Y_{ijk}^{(\,)}$ in Fig. 3 may be expressed by

$$Y_{11k}^{(\,)} = Y_{F11k}^{(\,)} - j\frac{Y_{F12k}^{(\,)}Y_{F21k}^{(\,)}Z_{Dk}^{(\,)}\tan\theta_{Dk}^{(\,)}}{1+jY_{F22k}^{(\,)}Z_{Dk}^{(\,)}\tan\theta_{Dk}^{(\,)}} \tag{1a}$$

$$Y_{12k}^{(\,)} = \frac{Y_{F12k}^{(\,)}}{\cos\theta_{Dk}^{(\,)} + jY_{F22k}^{(\,)}Z_{Dk}^{(\,)}\sin\theta_{Dk}^{(\,)}} \tag{1b}$$

$$Y_{21k}^{(\,)} = \frac{Y_{F21k}^{(\,)}}{\cos\theta_{Dk}^{(\,)} + jY_{F22k}^{(\,)}Z_{Dk}^{(\,)}\sin\theta_{Dk}^{(\,)}} \tag{1c}$$

$$Y_{22k}^{(\,)} = Y_{Dk}^{(\,)} + \frac{1}{Z_{Dk}^{(\,)}}\frac{Y_{F22k}^{(\,)}Z_{Dk}^{(\,)} + j\tan\theta_{Dk}^{(\,)}}{1+jY_{F22k}^{(\,)}Z_{Dk}^{(\,)}\tan\theta_{Dk}^{(\,)}}. \tag{1d}$$

Here the $Y_{Fijk}^{(\,)}$ represent the admittance parameters of the active devices. (Note that for practical reasons the drain line stub admittance of the first tier has been set to $Y_{Dk}^{(A)}=0$ in the schematics of Figs. 1 and 2.)

0018-9480/88/0100-0011$01.00 ©1988 IEEE

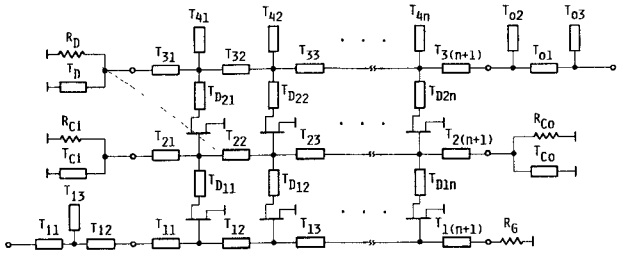

DESCRIPTION OF CIRCUIT COMPONENTS

- T_{in} - INPUT MATCHING TRANSMISSION LINE ELEMENTS
- T_{on} - OUTPUT MATCHING TRANSMISSION LINE ELEMENTS
- T_{1k} - GATE LINE TRANSMISSION LINE ELEMENTS
- T_{2k} - CENTER LINE TRANSMISSION LINE ELEMENTS
- T_{3k} - DRAIN LINE TRANSMISSION LINE ELEMENTS
- T_{D1k} - TRANSFORMING TRANSMISSION LINE ELEMENTS (1. TIER)
- T_{D2k} - TRANSFORMING TRANSMISSION LINE ELEMENTS (2. TIER)
- T_{4k} - DRAIN LINE OPEN-CIRCUIT SHUNT STUBS
- R_G - GATE LINE TERMINATION
- $R_{ci,o}$ - CENTER LINE TERMINATIONS
- R_D - DRAIN LINE TERMINATION
- $T_{ci,o}$ - CENTER LINE SHORT-CIRCUIT SHUNT STUBS
- T_D - DRAIN LINE SHORT-CIRCUIT SHUNT STUB

Fig. 1. Schematic of the two-tier matrix amplifier with n active six-ports.

In accordance with the equivalent circuit of Fig 3, which takes into consideration the transformations and capacitive loading expressed by (1), we are now in a position to find the voltages and currents at the gate line, the center line, and the drain line of our active six-port. They may be written in the form of the chain matrix equation

$$\begin{bmatrix} V_{Dk-1} \\ I_{Dk-1} \\ \hline V_{Ck-1} \\ I_{Ck-1} \\ \hline V_{Gk-1} \\ I_{Gk-1} \end{bmatrix} = \mathbf{A}_{Fk} \begin{bmatrix} V_{Dk} \\ -I_{Dk} \\ \hline V_{Ck} \\ -I_{Ck} \\ \hline V_{Gk} \\ -I_{Gk} \end{bmatrix} + \mathbf{B}_{Fk} \begin{bmatrix} -v_k^{(B)} \\ i_k^{(B)} \\ \hline -v_k^{(A)} \\ i_k^{(A)} \\ \hline 0 \\ 0 \end{bmatrix} \tag{2}$$

where

$$\mathbf{A}_{Fk} = \left[\begin{array}{cc|cc|cc} 1 & 0 & 0 & 0 & 0 & 0 \\ Y_{22k}^{(B)} & 1 & Y_{21k}^{(B)} & 0 & 0 & 0 \\ \hline 0 & 0 & 1 & 0 & 0 & 0 \\ Y_{12k}^{(B)} & 0 & \left(Y_{11k}^{(B)} + Y_{22k}^{(A)}\right) & 1 & Y_{21k}^{(A)} & 0 \\ \hline 0 & 0 & 0 & 0 & 1 & 0 \\ 0 & 0 & Y_{12k}^{(A)} & 0 & Y_{11k}^{(A)} & 1 \end{array}\right] \tag{2a}$$

$$\mathbf{B}_{Fk} = \left[\begin{array}{cc|cc|cc} 0 & 0 & 0 & 0 & 0 & 0 \\ Y_{21k}^{(B)} & 0 & 0 & 0 & 0 & 0 \\ \hline 0 & 0 & 0 & 0 & 0 & 0 \\ Y_{11k}^{(B)} & 1 & Y_{21k}^{(A)} & 0 & 0 & 0 \\ \hline 0 & 0 & 0 & 0 & 0 & 0 \\ 0 & 0 & Y_{11k}^{(A)} & 1 & 0 & 0 \end{array}\right]. \tag{2b}$$

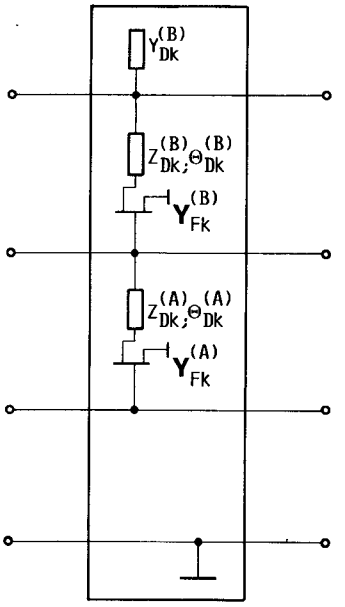

Fig 2. The two-tier active six-port.

$[A_{Fk}]$ is designated the signal matrix of our active six-port, while $[B_{Fk}]$ is its noise matrix. The latter transforms the transistors' internal noise sources to the three input ports of the elementary six-port. The transmission line elements connected to each output of the two transistors in Fig. 2 change the noise currents of the subcircuit in accordance with (2b) of the chain matrix equation (2). The voltages and currents of (2) contain both the signal and the noise components. As the amplification process of the signal has already been discussed in detail in a previous paper [1] and, therefore, will not concern us any longer, we now separate the signal from the noise quantities. This can be easily accomplished since the amplifier is always assumed to operate under linear conditions, where total voltages and currents are simply the sum of their signal and noise components. The noise parameters, which are symbolized by lower case letters, may be expressed by

$$\begin{bmatrix} v_{Dk-1} \\ i_{Dk-1} \\ \hline v_{Ck-1} \\ i_{Ck-1} \\ \hline v_{Gk-1} \\ i_{Gk-1} \end{bmatrix} = \mathbf{A}_{Fk} \begin{bmatrix} v_{Dk} \\ -i_{Dk} \\ \hline v_{Ck} \\ -i_{Ck} \\ \hline v_{Gk} \\ -i_{Gk} \end{bmatrix} + \mathbf{B}_{Fk} \begin{bmatrix} -v_k^{(B)} \\ i_k^{(B)} \\ \hline -v_k^{(A)} \\ i_k^{(A)} \\ \hline 0 \\ 0 \end{bmatrix}. \tag{3}$$

In physical terms, (3) transforms all noise voltages and currents appearing at the output of our six-port $(v_{Dk}, i_{Dk}, v_{Ck}, i_{Ck}, v_{Gk}, i_{Gk})$ and all of its internal noise sources $(v_k^{(B)}, i_k^{(B)}, v_k^{(A)}, i_k^{(A)})$ to the input of the device rendering the two-tier active six-port itself and all circuitry connected to its output terminals noiseless.

B. The Amplifier

When dealing with the entire amplifier, the unit's boundary conditions need to be taken into consideration.

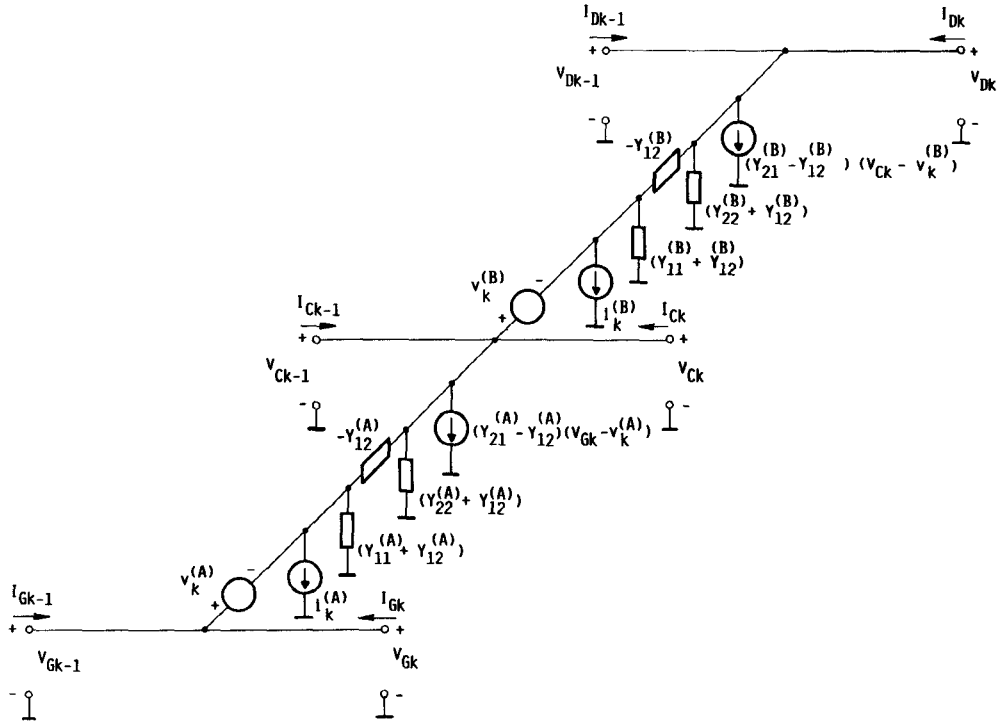

Fig. 3. Equivalent circuit of the active six-port including its internal noise sources.

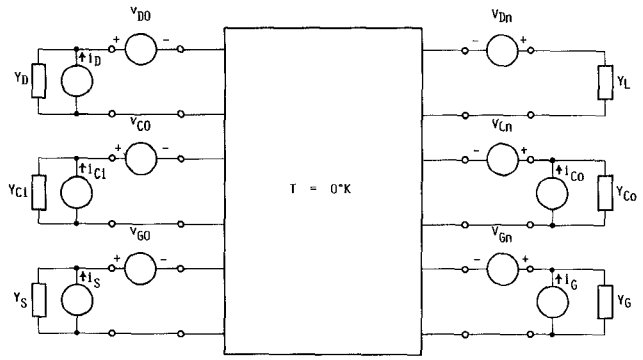

Fig. 4. Termination conditions and external noise sources of the matrix amplifier.

As demonstrated in Fig. 4, the matrix amplifier's four idle ports are terminated with the admittances Y_D at the drain line, Y_{C_i} and Y_{C_o} at the two ports of the center line, and Y_G at the gate line. The signal source with its internal admittance Y_S is connected to the amplifier's input terminal, while the amplifier's output power is delivered to the load admittance Y_L. In general, all six terminations contain a finite conductance, each injecting noise into the network. Except for the load admittance Y_L, which is not part of the amplifier, all other terminations (Y_S, Y_G, Y_{C_i}, Y_{C_o}, and Y_D) contribute to the noise power that is delivered to the amplifier's output terminal. In most cases, the active devices' noise components outweigh those of the terminations, especially at high frequencies. Their magnitudes may be determined with (3) and represented by the noise voltage sources v_{D0}, v_{C0}, v_{G0}, v_{Dn}, v_{Cn}, and v_{Gn} at each of the six terminal pairs in Fig. 4. As already pointed out, this is accomplished by transforming the active devices' noise sources to the six-port terminals, as illustrated in Fig. 4, rendering the six-port free of noise. The two-tier active six-ports of Figs. 2 and 3 are linked with a network of inductances or, as is the case in Fig. 1, of transmission line elements. They may conveniently be represented by the six-ports that are described in [1]. Through multiplication of the elementary six-port matrices in the sequence they are cascaded, all noise contributed by any active device or lossy component, such as a termination, will be transformed to the amplifier's input terminals. Finding then the relationship that exists between the internal noise sources and the transformed noise voltages representing the former at the amplifier's terminals becomes now an exercise in matrix algebra.

Applying the boundary conditions as they are defined in Fig. 4 to the amplifier and assuming n active six-ports, we derive the following matrix equation:

$$\begin{bmatrix} v_{D0} \\ -(Y_D v_{D0} - i_D) \\ v_{C0} \\ -(Y_{C_i} v_{C0} - i_{C_i}) \\ v_{G0} \\ -(Y_s v_{G0} - i_s) \end{bmatrix} = \mathbf{A} \begin{bmatrix} v_{Dn} \\ Y_L v_{Dn} \\ v_{Cn} \\ (Y_{C_o} v_{Cn} - i_{C_o}) \\ v_{Gn} \\ (Y_G v_{Gn} - i_G) \end{bmatrix} + \sum_{k=1}^{n} \left\{ \mathbf{E}_k \begin{bmatrix} -v_k^{(B)} \\ i_k^{(B)} \\ -v_k^{(A)} \\ i_k^{(A)} \\ 0 \\ 0 \end{bmatrix} \right\} \quad (4)$$

where

$$\mathbf{A} = \mathbf{A}_i \left\{ \prod_{k=1}^{n+1} \mathbf{A}_k \right\} \mathbf{A}_o \tag{4a}$$

$$\mathbf{E}_k = \mathbf{A}_i \left\{ \prod_{m=1}^{k-1} A_m \right\} A_k^I B_{Fk} \tag{4b}$$

$$\mathbf{A}_k = \mathbf{A}_k^I \mathbf{A}_k^{II} \tag{4c}$$

$$\mathbf{A}_{n+1}^{II} = \mathbf{I}. \tag{4d}$$

$[A_i]$ and $[A_o]$ are the matrices of the input and output matching networks, respectively, while $[A_k^{II}]$ represents the kth active six-port and $[A_k^I]$ the linking six-port preceding the former. The final linking six-port following the last active device is characterized by $[A_{n+1}^I]$. The links are numbered in the sequence they are cascaded beginning at the input end. As is the case for the linking six-ports, the input and output matching network's matrix can be found in [1].

The matrix equation (4) expresses the relationship between the input and output noise parameters. Unfortunately, the unknown voltages $(v_{D0}, v_{C0}, v_{G0}, v_{Dn}, v_{Cn}, v_{Gn})$ still appear on both sides of the equation, as do the known quantities $(i_D, i_{Ci}, i_S, i_{Co}, i_G, v_k^{(B)}, v_k^{(A)}, i_k^{(B)}, i_k^{(A)})$; i.e., the result is in implicit form. Formulating the unknown voltages as functions of the known quantities requires a significant amount of restructuring, which is quite involved and rather tedious. We therefore refer the interested reader to the Appendix for the results of these efforts.

Before proceeding any further, the assumption is made that no correlation exists between any noise voltages and noise currents except if they originate in one and the same device, as is the case in our transistors. The correlation is expressed by

$$i_k = i_{nk} + (Y_{\text{cor}})_k v_k \tag{5}$$

which gives us the relationship between that part of the current i_k, namely i_{nk}, that is not correlated with the voltage v_k. $(Y_{\text{cor}})_k$ is the well-known correlation admittance of the kth device [4].

Using (4) and the F parameters determined in the Appendix, we may now formulate the amplifier's output noise voltage v_{Dn} appearing across the load Y_L as a function of all noise sources present:

$$\begin{aligned} v_{Dn} = {} & Q_1 i_D + Q_2 i_{Ci} + Q_3 i_s + Q_4 i_{Co} + Q_5 i_G \\ & + \sum_{k=1}^{n} \left[\left(Q_6 - Y_{\text{cor}}^{(B)} Q_8 \right)_k v_k^{(B)} + \left(Q_7 - Y_{\text{cor}}^{(A)} Q_9 \right)_k v_k^{(A)} \right] \\ & - \sum_{k=1}^{n} \left[Q_{8k} i_{nk}^{(B)} + Q_{9k} i_{nk}^{(A)} \right]. \end{aligned} \tag{6}$$

The dependence of the Q parameters on F_1, F_2, and F_3 and the circuit parameters E_{ij} as well as the admittances at the input and output ports, Y_D, Y_{Ci}, Y_S, Y_L, Y_{Co} and Y_G, may also be obtained from the Appendix.

In compliance with Fig. 4, the unit delivers the noise output power

$$N_{Dn} = Y_L \overline{|v_{Dn}|^2} \tag{7}$$

to the load Y_L.

Consistent with (5) and (6), we have

$$\begin{aligned} \overline{|v_{Dn}|^2} = {} & |Q_1|^2 \overline{|i_D|^2} + |Q_2|^2 \overline{|i_{Ci}|^2} + |Q_3|^2 \overline{|i_s|^2} + |Q_4|^2 \overline{|i_{Co}|^2} \\ & + |Q_5|^2 \overline{|i_G|^2} \\ & + \sum_{k=1}^{n} \left[|Q_6 - Y_{\text{cor}}^{(B)} Q_8|_k^2 \overline{|v^{(A)}|_k^2} \right. \\ & \left. + |Q_7 - Y_{\text{cor}}^{(A)} Q_9|_k^2 \overline{|v^{(B)}|_k^2} \right] \\ & + \sum_{k=1}^{n} \left[|Q_8|_k^2 \overline{|i^{(B)}|_k^2} + |Q_9|_k^2 \overline{|i^{(A)}|_k^2} \right]. \end{aligned} \tag{8}$$

The available noise input power generated by the source is

$$N_S = kT_0 \Delta f \tag{9}$$

where k is Boltzmann's constant.

Using the well-known Nyquist formulas

$$\overline{|i|^2} = 4kT_0 G \Delta f \tag{10a}$$

$$\overline{|v|^2} = 4kT_0 R \Delta f \tag{10b}$$

we now are able to determine the amplifier's gain with (7)–(10):

$$\text{GAIN} = 4G_S Y_L |Q_3|^2. \tag{11}$$

Here G_S is the source conductance.

Since the input noise power (9), the output noise power (7), and the gain (11) are now known, we are finally in a position to determine the two-tier matrix amplifier's noise figure. Using the Nyquist formulas (10), it is

$$\begin{aligned} NF = 1 + \frac{1}{G_s |Q_3|^2} \Bigg[& |Q_1|^2 G_D + |Q_2|^2 G_{Ci} + |Q_4|^2 G_{Co} + |Q_5|^2 G_G \\ & + \sum_{k=1}^{n} \left(|Q_6 - Y_{\text{cor}}^{(B)} Q_8|_k^2 R_{nk}^{(B)} + |Q_7 \right. \\ & - Y_{\text{cor}}^{(A)} Q_9|_k^2 R_{nk}^{(A)} + |Q_8|_k^2 G_{nk}^{(B)} \\ & \left. + |Q_9|_k^2 G_{nk}^{(A)} \right) \Bigg]. \end{aligned} \tag{12}$$

Equation (12) not only enables us to compute the noise figure, but also makes it possible to trace it to the individual components which inject the noise. Such insight, of course, is of great value for understanding and, eventually, optimizing the noise figure of the matrix amplifier. In the next section when the noise of a variety of amplifiers is quantitatively studied, we will take advantage of this attribute in order to spot the main contributors to the device's noise figure.

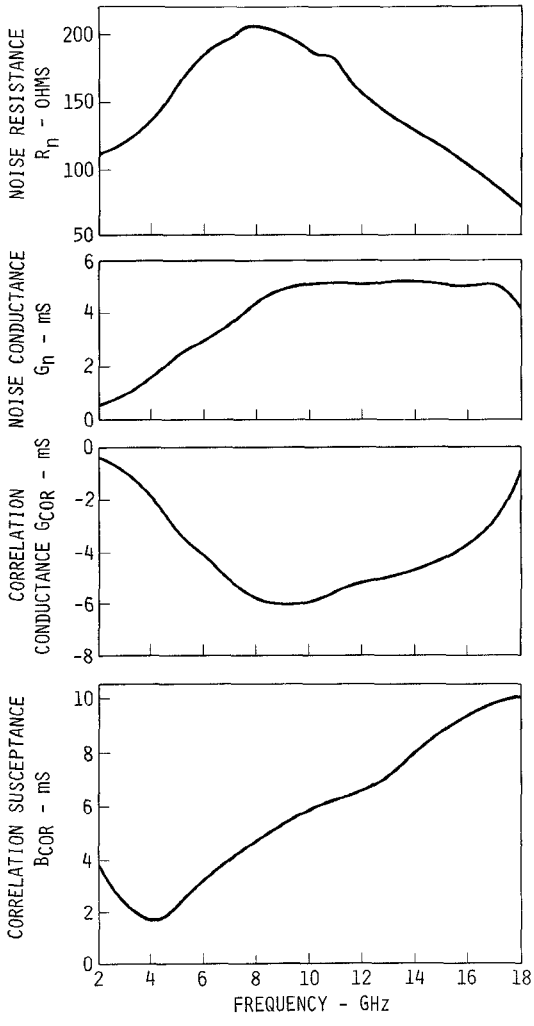

Fig. 5. The equivalent noise parameters of the active devices processed on ion-implanted material.

III. Comparison of Computed Performance Characteristics

In this chapter we will discuss the computed performance characteristics of the two-tier matrix amplifier, such as the small-signal gain (11), the noise figure (12), and the reflection coefficients. The latter may be determined with [1, eq. (A7)] or, of course, any computer program based on nodal analysis. Before becoming involved with the analysis, we need to characterize our active devices. For practical reasons, the use of identical devices in all positions of both tiers was chosen. Their equivalent circuit, with the exception of the transconductance $g_m = 26.5$ mS, is identical to that described in [1]. The reduction of g_m from 29.7 mS in [1] to 26.5 mS in this study was necessary in order to bring gains measured on a number of amplifiers into closer agreement with the computed results. The noise parameters characterizing a single representative of the MESFET's employed in the experimental amplifier of [1] are plotted in Fig. 5.

From the noise theory of the distributed amplifier [3], we have learned that the noise figure in the lower portion of the frequency band decreases with increasing number of

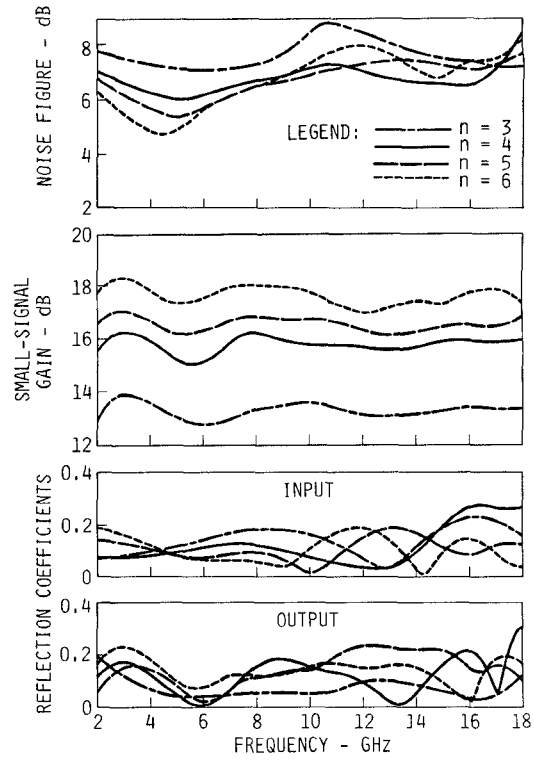

Fig. 6. Dependence of the performance parameters on the number of active six-ports n.

active links. Hence, the question arises whether we can expect similar behavior from the two-tier matrix amplifier. In addition, and analogous to the distributed amplifier, we anticipate an improvement in the gain with n without sacrificing the input and output match. In order to make the comparison between amplifiers of various numbers of active links meaningful, all passive circuit elements are optimized for gain, gain flatness, and VSWR. The schematic of the circuit to be analyzed is that of Fig. 1. The optimization, as will be seen in the next section when we discuss an experimental amplifier, leads to unequal links of the "declining drain line lengths" variety [5]. The results of our computations are reflected in Fig. 6, which compares the noise figure, the gain, and the reflection coefficients of the two-tier matrix amplifier for $n = 3$, 4, 5, and 6 active six-ports. The improvements of the noise figure at low frequencies and of the gain across the entire frequency band are clearly discernible. As can be seen, the magnitudes of the input and output reflection coefficients remain within acceptable limits.

From the computed data shown in Fig. 6, it seems that the unit with $n = 5$ active six-ports represents a good compromise between complexity and overall performance and is therefore a good vehicle on which to continue our studies. But before we do so, let us briefly examine which group of noisy elements has the greatest influence on the amplifier's noise performance at any particular frequency. Again we conduct this study for different numbers of active links n. The outcome of our computations is plotted in Fig. 7, which shows the noise contributions of the first and second tiers of transistors as well as that of all

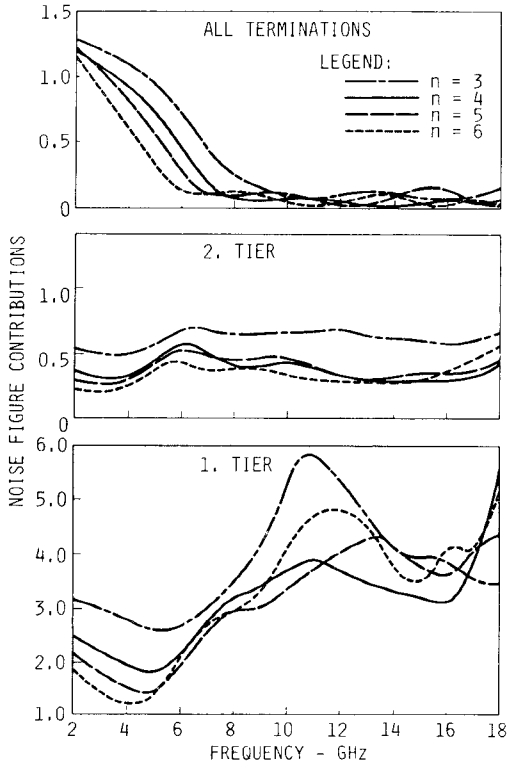

Fig. 7. Noise figure contributions due to the first and second tiers of transistors as well as all terminations for $n = 5$.

terminations combined to the total noise figure F. Note that the results are expressed in numeric, rather than logarithmic, figures. They add up to the numeric excess noise figure of the amplifier, i.e., $(F-1)$. The terminations' influence on noise figure declines with frequency and, for the most part, with the number of active six-ports n at frequencies up to about $f = 7$ GHz. Beyond $f = 10$ GHz their contribution is practically negligible. As expected, the first tier of active devices contributes the largest portion of noise while the noise contribution of the second tier is only a small fraction of that of the first tier. As will be demonstrated in the next section, for a practical design ($n = 4$), between approximately 50 percent and 87 percent of the terminations' noise is injected by the gate termination and hardly any by the drain termination. That immediately, though not unexpectedly, singles out the gate resistance R_G as the dominant noise contributor outside of the active devices. Therefore, reducing the amplifier's overall noise figure by altering the gate resistance R_G becomes an important design tool when low-noise performance is of major concern. Obviously, such a change will impair other performance parameters such as gain, gain flatness, and VSWR. Hence, any change in R_G requires a reoptimization of all circuit parameters to at least preserve an acceptable gain performance. Fortunately, the latter can be accomplished when we include the admittances of the remaining three terminations Y_{Ci}, Y_{Co} and Y_D into the optimization process. The resulting performance characteristics of the amplifier for $n = 5$ are presented in Fig. 8 for different values of R_G. As is easily discernible, the gain flatness and VSWR's can be held at acceptable levels if the

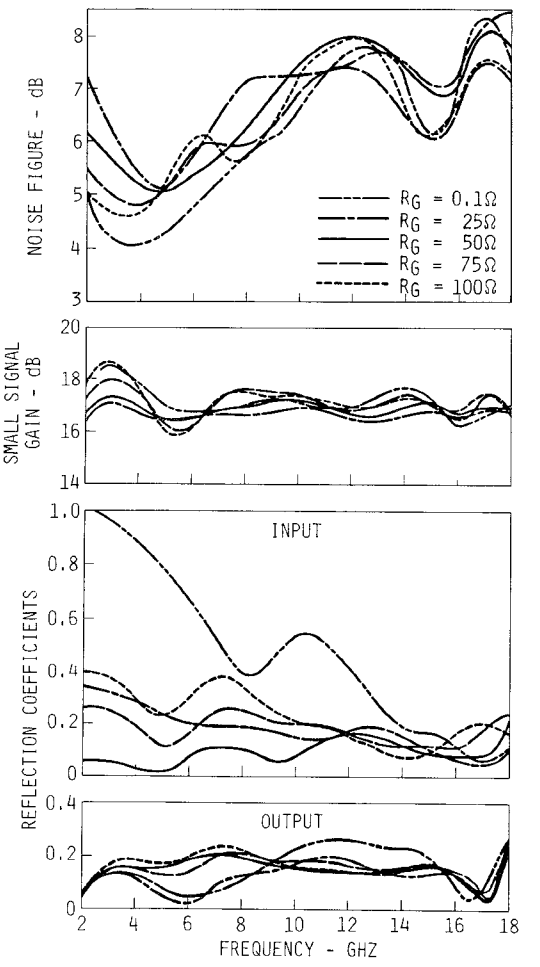

Fig. 8. The influence of the gate resistance R_G on noise figure, small-signal gain, and reflection coefficients for $n = 5$.

values of R_G are chosen within reasonable limits ($25\ \Omega \leq R_G \leq 100\ \Omega$). Naturally, this is not the case at $R_G = 0.1\ \Omega$, for which the module exhibits unstable operation at frequencies below approximately $f = 2.4$ GHz. Within the range of acceptable performance parameters, $R_G = 50\ \Omega$ emerges as the logical choice for the best overall performance. It is worth mentioning that for $0.1\ \Omega \leq R_G \leq 100\ \Omega$, the gain performance may be retained within the limits shown in Fig. 8 by simply optimizing the remaining termination resistors and all other passive circuit elements for gain flatness and VSWR. The resulting ranges of the termination resistors are $25\ \Omega < R_{Ci} < 50\ \Omega$, $10\ \Omega < R_{Co} < 50\ \Omega$, and $65\ \Omega < R_D < 120\ \Omega$.

This section would not be complete without a comparison of the noise figures of the matrix amplifier and its equivalent two-stage distributed amplifier. In our case, equivalence means the employment of identical types and numbers of devices in both units, which are optimized for best gain and VSWR performance. Since our experimental amplifier, which will be discussed in the following section, uses $n = 4$ active six-ports, i.e., eight GaAs MESFET's, we will conduct this study for $n = 4$. Consequently, the equivalent two-stage distributed amplifier employs $n = 4$ transistors in each of its two identical modules. The results of our computations are displayed in Fig. 9. The small-signal

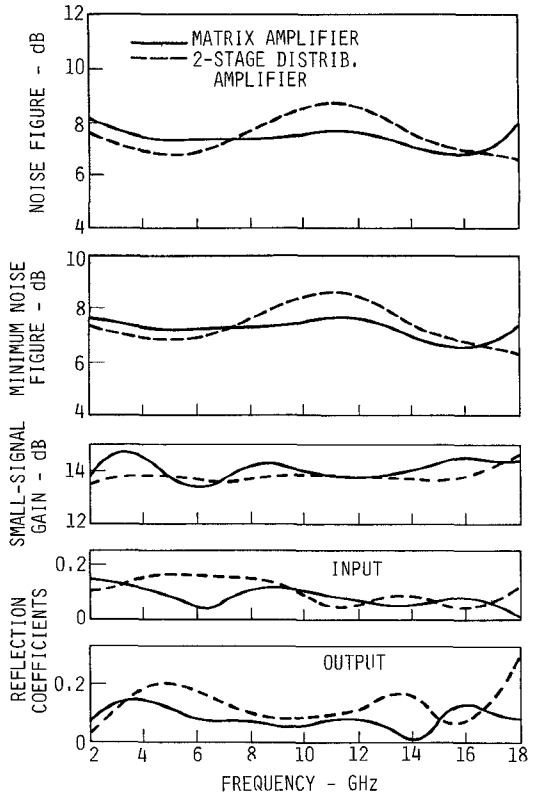

Fig. 9. Performance comparison of the $n = 4$ two-tier matrix amplifier with the equivalent $n = 4$ two-stage distributed amplifier.

gain flatness of the two-stage distributed amplifier is definitely smoother, and its input reflection coefficient is roughly of the same quality as that of the matrix amplifier. The latter's output match as well as its overall noise figure, however, due to its lower maximum noise figure across the frequency band, is clearly preferable. While in this case the difference between the maximum noise figures of the equivalent gain amplifiers is only 0.6 dB we have found examples where it differs in excess of 2 dB when the noise figure is included in the optimization process.

While this outcome is encouraging, it does not represent sufficient evidence to favor one concept over the other as far as noise performance is concerned. Much research, far beyond the scope of this paper, is needed to produce convincing proof on the subject of noise figure superiority. However, until now we have not found a schematic for an equivalent two-stage distributed amplifier that disputes the tendencies demonstrated in Fig. 9.

IV. Experimental Results

At first, we will compare the computed results with the measured data, obtained from an $n = 4$ two-tier matrix amplifier in accordance with the schematic of Fig. 1 and described in a previous paper [1]. For reasons explained earlier, the transconductance of the GaAs MESFET's was reduced from $g_m = 29.7$ mS in [1] to $g_m = 26.5$ mS. All other parameters of either the transistors' equivalent circuit or the matrix amplifier itself are identical to those in [1]. It is important to note that none of the discussed

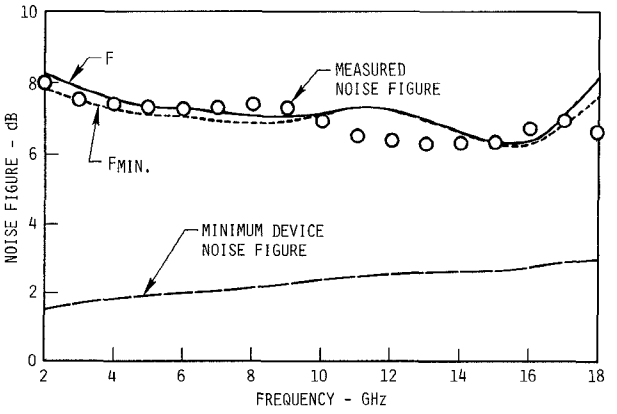

Fig. 10. Comparison of the measured and computed noise figure of the amplifier (the computed minimum noise figures of the amplifier and the devices also being shown).

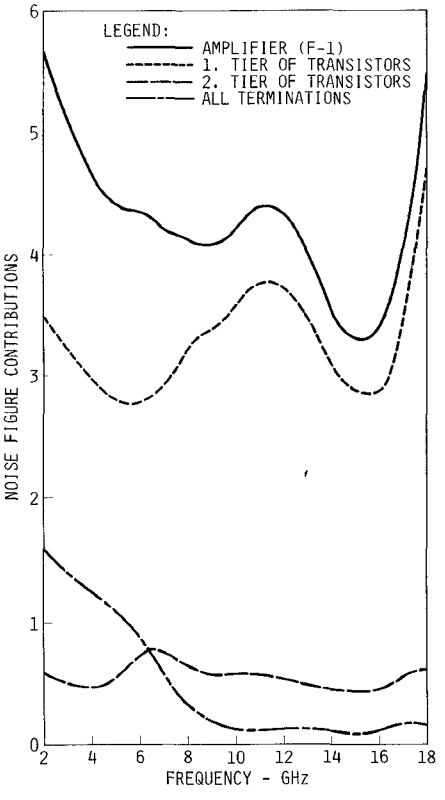

Fig. 11. The major sources contributing to the overall noise figure of the $n = 4$ two-tier matrix amplifier.

measures to reduce the noise by compromising between noise figure, VSWR, and gain flatness were quantitatively known at the time of this amplifier's design. The device was optimized for gain, gain flatness, and VSWR without any consideration for noise figure.

Fig. 10 compares the noise figure computed with (12) and the data measured on the amplifier when the devices characterized by the noise parameters of Fig. 5 were incorporated. As is the case for the distributed amplifier, there is little difference between the noise figure and the minimum noise figure of the two-tier matrix amplifier. In Fig. 11 we have broken out the major sources contributing to the noise. The components, like those in Fig. 7, are numeric

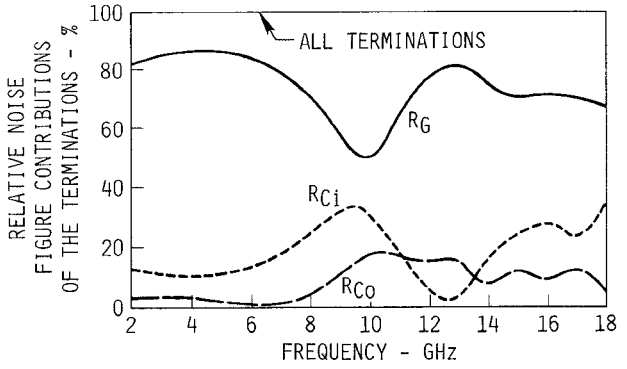

Fig. 12. Relative numeric noise contributions of the terminations of the $n = 4$ two-tier matrix amplifier.

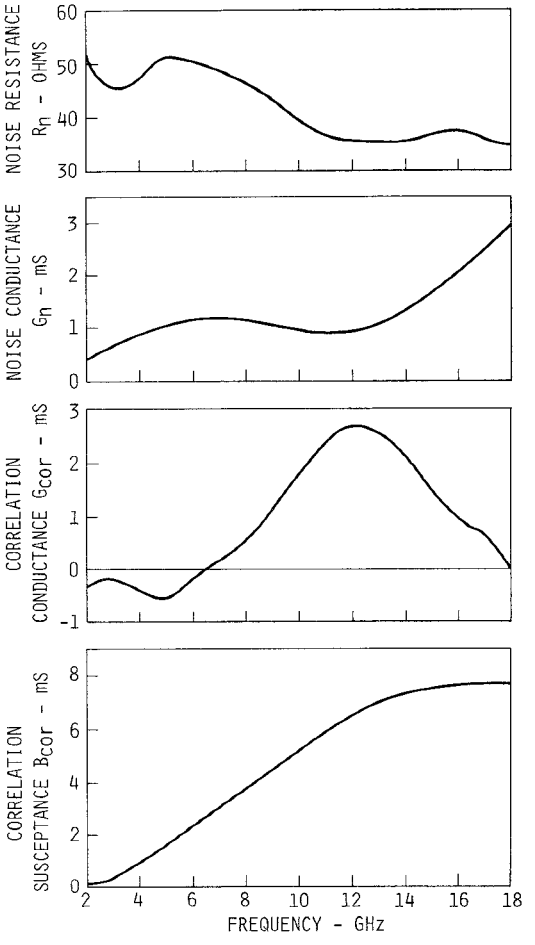

Fig. 13. The equivalent noise parameters of the active devices processed on VPE material.

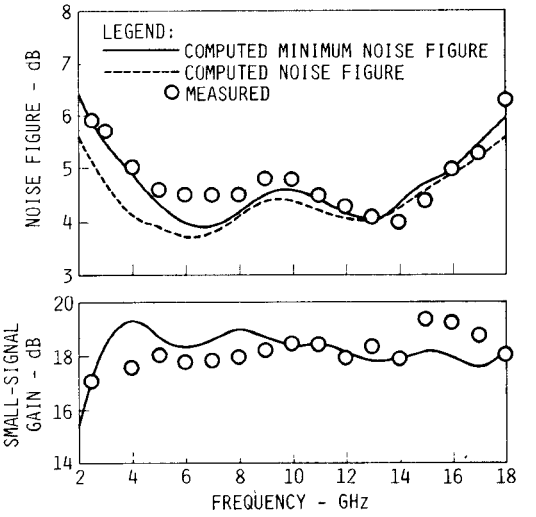

Fig. 14. Comparison of the measured and computed data of the amplifier in Fig. 1 ($n = 4$) when incorporating VPE transistors.

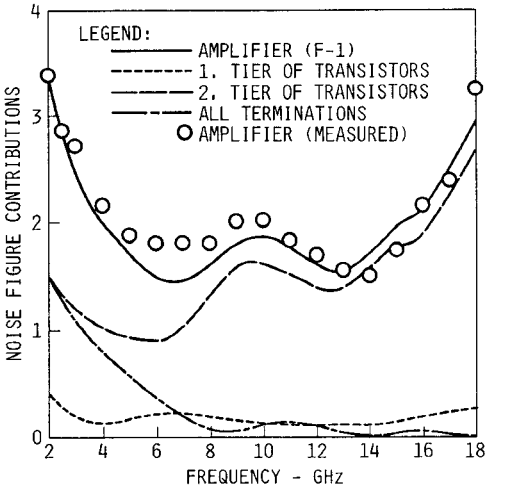

Fig. 15. Contributions of the individual noise sources to the numeric excess noise figure in case the VPE devices are employed.

and add up to the numeric excess noise figure $(F-1)$ of the amplifier. It can be easily seen that the noise contribution of the first tier dominates the amplifier's noise behavior and that above $f = 10$ GHz the terminations' participation in the overall noise figure becomes negligible. The contribution of the second tier never exceeds 20 percent of the amplifier's numeric excess noise figure. In Fig. 12 we pay attention to the terminations' noise only, which, as expected, is dominated by the gate termination. The contributions of the center line terminations are significantly lower, while that of the drain termination is mostly below 1 percent and therefore not shown.

A second amplifier, which employed GaAs MESFET's with a topology identical to that of the active devices discussed so far but processed on vapor phase epitaxial rather than the ion-implanted material used in the fabrication of the earlier MESFET's [1], was also tested. The devices' noise behavior is reflected in the curves of Fig. 13 and is significantly different from that of its ion-implanted counterpart represented by Fig. 5. A comparison of the computed and measured noise figures as well as the small-signal gains of this module is shown in Fig. 14. Across the 2.5–18.0-GHz frequency band, a maximum noise figure of $F = 6.3$ dB and a gain of $G = 18.3 \pm 1.1$ dB were recorded. Finally, in Fig. 15, the individual noise sources' contributions to the numeric excess noise figure are plotted. Again, the first tier's noise contribution dominates the amplifier's noise performance. In this case the maximum noise contribution of the second tier relative to that of the first is approximately 25 percent.

V. Conclusions

Formulas have been derived that permit the computation of the noise figure and the gain of the two-tier matrix amplifier consisting of n active six-ports. Using the formulas, the noise behavior of the amplifier as it depends on the device and circuit parameters was studied. As is the case for the distributed amplifier, the noise injected by the terminations decreases with frequency. Also, the noise figure at the low end of the band decreases with increasing number of active six-ports (n), analogous to the distributed amplifier, where it becomes smaller with the number of transistors. The first tier of active devices, as expected, is the chief contributor to the amplifier's noise. The participation of the terminations' noise becomes negligible at frequencies above $f = 10$ GHz while the second tier's noise component represents a relatively small fraction of the total noise. The latter deviates insignificantly from the noise buildup of the equivalent two-stage distributed amplifier whose first stage mostly dominates its noise figure. A significant outcome of our theoretical as well as experimental studies, although performed for specific GaAs MESFET's, is the matrix amplifier's lower noise figures over the high-frequency portion of the band in comparison to those of the equivalent distributed amplifier. Finding out about the conditions that constitute the limiting factors to this important result merits future analysis.

Appendix

Based on the boundary conditions as they are specified in Fig. 4, we have derived the matrix equation (4). It expresses the relationship, in implicit form, between the input and output noise voltages v_{D0}, v_{C0}, v_{G0}, v_{Dn}, v_{Cn}, and v_{Gn}. In order to obtain the noise voltage at the amplifier's output port v_{Dn} (6) as a function of the known noise quantities i_D, i_{Ci}, i_S, i_{Co}, i_G, $v_k^{(A)}$, $v_k^{(B)}$, $i_k^{(A)}$, and $i_k^{(B)}$, we need to compute the Q parameters of (6). Since this is a rather laborious, though elementary, procedure, the discourse of the interim steps is omitted and the discussion is confined to the presentation of the results.

With the matrix components A_{ij} of the amplifier module defined by (4a), we obtain

$$Q_1 = F_1 \tag{A1a}$$

$$Q_2 = F_2 \tag{A1b}$$

$$Q_3 = F_3 \tag{A1c}$$

$$Q_4 = F_1(A_{24} + Y_D A_{14}) + F_2(A_{44} + Y_{Ci} A_{34}) + F_3(A_{64} + Y_S A_{54}) \tag{A1d}$$

$$Q_5 = F_1(A_{26} + Y_D A_{16}) + F_2(A_{46} + Y_{Ci} A_{36}) + F_3(A_{66} + Y_S A_{56}) \tag{A1e}$$

$$Q_{6k} = F_1(E_{21} + Y_D E_{11})_k + F_2(E_{41} + Y_{Ci} E_{31})_k + F_3(E_{61} + Y_S E_{51})_k \tag{A1f}$$

$$Q_{7k} = F_1(E_{22} + Y_D E_{12})_k + F_2(E_{42} + Y_{Ci} E_{32})_k + F_3(E_{62} + Y_S E_{52})_k \tag{A1g}$$

$$Q_{8k} = F_1(E_{23} + Y_D E_{13})_k + F_2(E_{43} + Y_{Ci} E_{33})_k + F_3(E_{63} + Y_S E_{53})_k \tag{A1h}$$

$$Q_{9k} = F_1(E_{24} + Y_D E_{14})_k + F_2(E_{44} + Y_{Ci} E_{34})_k + F_3(E_{64} + Y_S E_{54})_k \tag{A1i}$$

where

$$F_1 = \frac{1}{F}(H_{33}H_{22} - H_{32}H_{23}) \tag{A2a}$$

$$F_2 = \frac{1}{F}(H_{32}H_{13} - H_{33}H_{12}) \tag{A2b}$$

$$F_3 = \frac{1}{F}(H_{23}H_{12} - H_{22}H_{13}) \tag{A2c}$$

and

$$F = H_{33}(H_{22}H_{11} - H_{12}H_{21}) + H_{32}(H_{21}H_{13} - H_{23}H_{11}) + H_{31}(H_{23}H_{12} - H_{22}H_{13}). \tag{A2d}$$

At last the H parameters are

$$H_{11} = (A_{21} + Y_L A_{22}) + Y_D(A_{11} + Y_L A_{12}) \tag{A3a}$$

$$H_{12} = (A_{23} + Y_{Co} A_{24}) + Y_D(A_{13} + Y_{Co} A_{14}) \tag{A3b}$$

$$H_{13} = (A_{25} + Y_G A_{26}) + Y_D(A_{15} + Y_G A_{16}) \tag{A3c}$$

$$H_{21} = (A_{41} + Y_L A_{42}) + Y_{Ci}(A_{31} + Y_L A_{32}) \tag{A3d}$$

$$H_{22} = (A_{43} + Y_{Co} A_{44}) + Y_{Ci}(A_{33} + Y_{Co} A_{34}) \tag{A3e}$$

$$H_{23} = (A_{45} + Y_G A_{46}) + Y_{Ci}(A_{35} + Y_G A_{36}) \tag{A3f}$$

$$H_{31} = (A_{61} + Y_L A_{62}) + Y_S(A_{51} + Y_L A_{52}) \tag{A3g}$$

$$H_{32} = (A_{63} + Y_{Co} A_{64}) + Y_S(A_{53} + Y_{Co} A_{54}) \tag{A3h}$$

$$H_{33} = (A_{65} + Y_G A_{66}) + Y_S(A_{55} + Y_G A_{56}). \tag{A3i}$$

The noise voltage at the unit's output port v_{Dn} is expressed by (6), and the noise output power N_{Dn} by (7). With (8)–(11), we are finally arriving at the formula for the noise figure (12).

Acknowledgment

The authors are indebted to R. R. Pereira, who performed the measurements and the tuning of the amplifier modules. In addition, they wish to thank J. L. Martin who assembled the circuits, as well as W. T. Wilser, whose department developed and fabricated the GaAs MESFET's used in these experiments and who edited this manuscript.

This paper is dedicated to Prof. H. Döring of the Technical University Aachen, W. Germany, who celebrated his 75th birthday in 1986 when this study was performed.

References

[1] K. B. Niclas and R. R. Pereira, "The matrix amplifier: A high-gain module for multioctave frequency bands," *IEEE Trans. Microwave Theory Tech.*, vol. MTT-35, pp. 296–306, Mar. 1987.

[2] V. Rizzoli and A. Lipparini, "Computer-aided noise analysis of linear multiport networks of arbitrary topology," *IEEE Trans. Microwave Theory Tech.*, vol. MTT-33, pp. 1507–1512, Dec. 1985.

[3] K. B. Niclas and B. A. Tucker, "On noise in distributed amplifiers at microwave frequencies," *IEEE Trans. Microwave Theory Tech.*, vol. MTT-31, pp. 661–668, Aug. 1983.
[4] H. Rothe and W. Dahlke, "Theory of noisy four-poles," *Proc. IRE*, vol. 44, pp. 811–818, June 1956.
[5] K. B. Niclas, R. D. Remba, R. R. Pereira, and B. D. Cantos, "The declining drain line lengths circuit—A computer derived design concept applied to a 2–26.5 GHz distributed amplifier," *IEEE Trans. Microwave Theory Tech.*, vol. MTT-34, pp. 427–435, Apr. 1986.

Karl B. Niclas (M'63–SM'80) received the Dipl. Ing. and Doctor of Engineering degrees from the Technical University of Aachen, Aachen, Germany, in 1956 and 1962, respectively.

From 1956 to 1962, he was with the Microwave Tube Laboratory at the Telefunken G.m.b.H. Tube Division, Ulm-Donau, Germany. He was engaged in research and development on ultra-low-noise and medium-power traveling-wave tubes. In 1958, he became Head of the company's Traveling-Wave Tube Section and Assistant Manager of the Microwave Tube Laboratory. From 1962 to 1963, he was associated as a Senior Project Engineer with the General Electric Microwave Laboratory, Stanford, CA. His work was mainly concerned with theoretical and experimental investigations of single-reversal focused low-noise traveling-wave tube amplifiers and resulted in the first lightweight amplifier of this type. In 1963, he joined the Technical Staff of Watkins-Johnson Company, Palo Alto, CA, and is presently Manager, Advanced Development, Devices Group. His current research efforts are primarily focused on advanced GaAs FET amplifiers and solid-state memory loop amplifiers. From 1967 to 1976, he was Manager of the company's Tube Division. Before that, he was Head of the Low-Noise Tube R&D Section, and prior to that he was engaged in a research program on new concepts for achieving high efficiency in traveling-wave tubes. He is the author of numerous papers in the fields of GaAs FET amplifiers, traveling-wave tubes, and electromagnetic field theory, and he holds a number of patents.

Dr. Niclas is the corecipient of the 1962 Outstanding Publications Award of the German Society of Radio Engineers (NTG) and the 1985 Microwave Prize awarded by the Microwave Theory and Techniques Society of the IEEE.

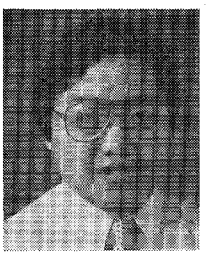

Augustin P. Chang (S'83–M'87) was born in Taiwan, Republic of China, on September 15, 1962. He received the B.S. degree in electrical engineering from Carnegie-Mellon University, Pittsburgh, PA, in 1984, and the M.S. degree in electrical engineering from the University of Illinois, Urbana-Champaign, in 1986.

In 1986, he joined the Technical Staff of the Watkins-Johnson Company, Palo Alto, CA, where he has been working on the development of state-of-the-art multioctave amplifiers. His research interests are in the area of large-signal modeling of MESFET's and monolithic microwave integrated circuit design.

Mr. Chang is a member of Eta Kappa Nu.